Strongly coupled quantum dot-metal nanoparticle systems: Exciton-induced transparency, discontinuous response, and suppression as driven quantum oscillator effects

Ryan D. Artuso*
Joint Quantum Institute and Department of Physics, University of Maryland, College Park, Maryland 20742-4111, USA

Garnett W. Bryant
Joint Quantum Institute and Atomic Physics Division, National Institute of Standards and Technology, Gaithersburg, Maryland 20899-8423, USA

(Received 7 July 2010; revised manuscript received 22 September 2010; published 9 November 2010)

We probe the transition to bistability that exists in a hybrid metal nanoparticle and semiconductor quantum dot (SQD) system when they are strongly coupled. In particular, we see a discontinuous jump in the response of the system (in both the diagonal and off-diagonal density-matrix elements) and a SQD response that is highly suppressed above resonance in this transition region. This discontinuous response and suppression arise because the SQD acts as a driven (quantum) oscillator. The phase change at resonance drastically alters the hybrid response when crossing the resonance. The study of this transition region, the discontinuity, and the suppression phenomena provides different insights into understanding this system, predicts a more complicated behavior than previously thought and corrects earlier work where the transition region was absent.

DOI: 10.1103/PhysRevB.82.195419 PACS number(s): 78.67.−n

I. INTRODUCTION

Transmission of quantum information between qubits for quantum communication, quantum computing, and quantum measurement will require transfer where the quantum character of the information can be maintained. Since diffraction-limited waveguiding of light will only give wavelength scale resolution, which will not be adequate for site-to-site nanoscale transmission, what is needed is directed transmission. One paradigm proposes to achieve directed nanoscale information transfer by coupling qubits, for example, in quantum dots (QDs), to plasmonic structures. This can be done over relatively long distances with dielectric nanoguides[1] and over submicron distances with nanoantennas or nanoguides made from metallic nanowires and nanoparticles.[2] At submicron distances, the losses in metallic nanoparticles should not be sufficient to destroy the quality of the information. Such hybrid nanoscale structures should allow for the physical transportation of excitations as well as the transportation of coherent states. These structures also stimulate the study of systems at the interface between classical and quantum physics and open up avenues to quantum nanooptics.

Advances in nanoscience have allowed for the construction of such nanosuperstructures. By using various combinations of available building blocks (nanowires, semiconductor quantum dots (SQDs), metal nanoparticles (MNPs), biolinkers, etc.) to create these superstructures, several physical phenomena have been explored. Recently, hybrid structures consisting of a quantum dot and a metal nanoparticle joined by a biolinker have been assembled and studied.[3] Furthermore, the radiative coupling of a CdSe quantum dot to a silver nanowire[4,5] and the polarization selective enhancement of quantum dot photoluminescence when coupled to metal nanoparticles[6] have been explored. Exciting results have been attained showing that quantum coherence can survive in plasmonic structures, such as the transportation of entangled photons by surface plasmons[7] and centimeter scale propagation of entangled plasmons[8,9] as well as the creation of a single plasmon in a temporal state of superposition.[8]

To exploit this paradigm for quantum, nanoscale communication, one must understand how metallic nanoparticles act as nanoantennas and nanoguides. One must understand the coupling between dots and plasmons in metallic nanoparticles. One must also understand how dot-to-dot quantum communication is modified by transfer via plasmons. Finally, one must understand how transfer is further modified if the metal nanoparticles are small and quantum effects can influence their response. Here we focus on the response of strongly coupled quantum dot/metal nanoparticle systems to understand how exciton-plasmon coupling will affect the transport of quantum information.

We discuss here, theoretically, the response of a hybrid nanostructure molecule consisting of a SQD and a MNP subject to an applied electric field (see Fig. 1). This system has been studied in the weak-coupling regime[10] and in the strong-coupling regime.[11] Similar systems have been studied with multiple metal nanoparticles,[12,13] with a nanowire instead of the spherical MNP (Ref. 14) and also with a metal-dielectric nanoshell.[15] The dipole-dipole coupling between two fluorescent molecules mediated by a chain of silver nanoparticles has also been studied.[16] Plasmon-induced

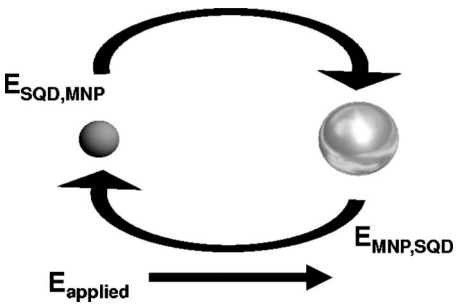

FIG. 1. An applied field polarizes both the MNP and SQD which in turn allows for a dipole-dipole coupling.

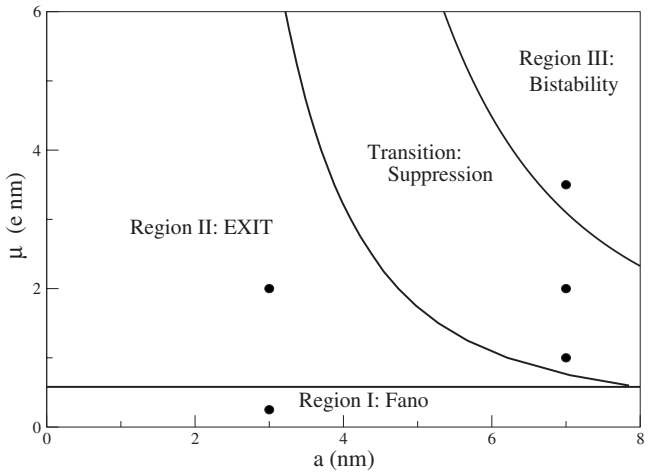

FIG. 2. μ vs a phase diagram for $R=13$ nm in the strong field limit. In addition to the three regimes of behavior previously discussed in Ref. 11, we find distinct phenomena in the transition between region II and region III. Points denote locations pictured in Figs. 3–5, 7, and 11.

transparency has been studied in a system consisting of a three level SQD interacting with a spherical MNP.[17]

The optical excitations of the SQD are the excitons, with a sharp, discrete response. The excitons act as quantum emitters. The strong, local, plasmonic excitations of the MNP provide a continuous spectrum of response. Enhanced local fields in the vicinity of the MNP provide strong coupling to neighboring SQDs. There is no direct tunneling between the MNP and SQD. However, due to the long-range Coulomb interaction, there is a dipole-dipole interaction that will allow them to couple and leads to excitation transfer.

The discrete excitons coupled with the broad response of the plasmons will allow for the appearance of exotic hybrid states and clear signatures for their optical response. As a damped driven oscillator, the SQD response to driving fields changes rapidly from in-phase to out-of-phase near the SQD resonance. Rapid variations in hybrid response are expected near the SQD resonance. Effects depending on the interference between applied and induced fields are extremely sensitive to this change from in-phase to out-of-phase SQD response, providing dramatic signatures from the hybrid response.

Previously, the weak field limit (driving field of 1 $\mathrm{W/cm^2}$) was studied.[10] The energy absorption spectrum shifts and broadens due to the coupling between the exciton in the SQD and the plasmon in the MNP. In the strong field limit (driving field of 100 $\mathrm{W/cm^2}$), local induced fields are comparable to the driving field. We find three regions of behavior as the SQD dipole moment, μ, and the radius of the MNP, a, are varied (see Ref. 11 and Fig. 2). The first region is for weak coupling between the MNP and SQD (small μ and small a). Here we see an asymmetrical Fano shape develop in the MNP energy absorption spectrum due to the interference at the MNP of the field from the SQD and the applied electric field.[10,11] As the SQD is increased in size (thus the coupling is increased), the asymmetrical Fano effect of region I is modified by the appearance of an additional peak with a deep minimum between the peaks.[11] Here, the induced local field at the MNP becomes larger than the applied field, for frequencies near the SQD resonance. As such, the interference of the field from the SQD with the applied electric field now results in a sign change in the net electric field at the MNP above resonance where the two fields are out-of-phase. An exciton-induced transparency (EXIT) arises in the MNP response when there is nearly complete destructive interference between these two fields acting on the MNP. When the MNP and SQD are further increased in size, there is an extreme broadening of the modified Fano shape that washes out the second peak. More interestingly, the response is nonlinear in this third regime. This nonlinearity is due to significant self-interaction of the SQD (feedback through the MNP). In this regime, there exists multiple steady-state solutions leading to a bistability with one of the stable solutions having a discontinuous absorption spectrum.[11]

We predicted in Ref. 11 that the transitions between regions were sharp. However this was an artifact of how we performed the calculations of the system response (as we discuss in Sec. II). When we reanalyzed the system dynamics, we find that regions I, II, and III are still clearly defined with the characteristics previously determined. However, the transition between regions is much more complicated than previously predicted, revealing additional complex behavior that determines the transition to bistability. Specifically, with proper accounting of the positive and negative frequency components of the driving and local fields, which was not done previously, we see that the transition between the regions II and III is a broad transition region (as shown in Fig. 2). In particular, in this transition region, we see a discontinuous jump in response of the system (in both the diagonal and off-diagonal density-matrix elements) as the driving frequency is varied. Moreover, the response of the SQD is highly suppressed above resonance in this transition region. The SQD responds as a damped oscillator, driven by the external field, the MNP field induced by the external field and the self-interaction mediated by the MNP. The self-interaction is determined by the SQD dipole moment. Below resonance the dipole moment of the SQD is in phase with the driving field and above resonance it is 180° out of phase. The phase of the self-interaction of the SQD is determined by the phase of dipole moment of the SQD, so there is destructive interference above resonance and constructive interference below resonance between the driving and the self interaction fields. Due to this interference, the SQD sees a weaker net electric field above resonance and its response is suppressed by the out-of-phase self-interaction. EXIT is determined by the interference between the fields that drive the MNP. Suppression is determined by the interference among the fields that drive the SQD. In both cases, the phase of some of the fields changes at resonance, leading to a crossover from constructive to destructive interference. The fields that do change phase at resonance originate from the phase change in the SQD dipole moment that occurs at resonance.

In Sec. II, we discuss the system in detail. We use a density-matrix approach to treat the SQD while the MNP is taken as a classical dielectric. We also calculate the energy absorption of the MNP and provide details on how numerical

calculations were carried out. In Sec. III we review the behavior of the system in regions I and II which were previously discussed in Ref. 11. In Sec. IV, we discuss the suppressed response of the SQD that occurs in the transition region between regions II and III. We also set bounds on parameter space in which the suppression occurs as well as connect this behavior to that of Region III. In Sec. V we analyze further the effects seen in region III, based on this distinct understanding of the transition region. Finally, we present our conclusions in Sec. VI.

II. SETUP

As in Refs. 10 and 11, we consider a spherical SQD with radius r interacting with a spherical MNP of radius a, separated by a distance R (as shown in Fig. 1). The entire system is subject to an applied electric field $E=E_0\cos(\omega t)$. We assume that all distances are small enough that retardation effects can be ignored and that the applied field is large enough that noise can be ignored. We treat the SQD quantum mechanically in the density-matrix formalism with exciton energy $\hbar\omega_0$, dipole moment μ, and dielectric constant ϵ_S. In the dipole limit only the three bright excitons (one for each optical axis) participate in the interaction. By choosing the direction of the applied field to be either perpendicular or parallel to the axis of our system, we in turn only excite one of the three excitons. Dark excitons do contribute to the exciton lifetime however. We treat the MNP as a classical spherical dielectric particle with dielectric function $\epsilon_M(\omega)$.

The Hamiltonian for the two level SQD, $\mathcal{H}_{\mathrm{SQD}}$, is

$$\mathcal{H}_{\mathrm{SQD}}=\hbar\omega_0\hat{a}^\dagger\hat{a}-\mu E_{\mathrm{SQD}}(\hat{a}+\hat{a}^\dagger), \tag{1}$$

where $\hat{a}$ and $\hat{a}^\dagger$ are the atomic, two-level operators representing exciton creation and annihilation. E_{SQD} is the total electric field felt by the SQD and consists of the applied, external field, E, and the induced, internal field, produced by the polarization of the MNP, $E_{\mathrm{MNP,SQD}}$. In the dipole limit, E_{SQD} is

$$E_{\mathrm{SQD}}=\frac{1}{\epsilon_{\mathrm{effS}}}\left(E+\frac{1}{4\pi\epsilon_B}\frac{s_\alpha P_{\mathrm{MNP}}}{R^3}\right), \tag{2}$$

where $\epsilon_{\mathrm{effS}}=\frac{2\epsilon_B+\epsilon_S}{3\epsilon_B}$ and $s_\alpha=2(-1)$ when the applied field is parallel (perpendicular) to the major axis of the system. ϵ_B is a background dielectric constant which would correspond to the substrate on which the system is placed. Being careful to separate out the negative and positive frequency contributions, the polarization of the MNP is (see Ref. 18),

$$P_{\mathrm{MNP}}=(4\pi\epsilon_B)a^3[\gamma\tilde{E}^{(+)}_{\mathrm{MNP}}e^{-i\omega t}+\gamma^*\tilde{E}^{(-)}_{\mathrm{MNP}}e^{i\omega t}].$$

$\tilde{E}^{(+)}_{\mathrm{MNP}}$ and $\tilde{E}^{(-)}_{\mathrm{MNP}}$ are the positive and negative frequency parts of the electric field felt by the MNP. Note that our choice of the sign convention is such that $\mathrm{Im}[\epsilon_m(\omega)]>0$ for $\omega>0$. The total field acting on the MNP, E_{MNP}, is just

$$E_{\mathrm{MNP}}=\left(E+\frac{1}{4\pi\epsilon_B}\frac{s_\alpha P_{\mathrm{SQD}}}{\epsilon_{\mathrm{effS}}R^3}\right), \tag{3}$$

where $\gamma=\frac{\epsilon_M(\omega)-\epsilon_B}{2\epsilon_B+\epsilon_M(\omega)}$. We make use of the density matrix ρ to calculate the polarization of the SQD. We label the ground state of our SQD (no exciton) as level 1 and the excited state (one exciton) we label as level 2. We then have $P_{\mathrm{SQD}}=\mu(\rho_{12}+\rho_{21})$ (see Ref. 19). Factoring out the high-frequency time dependence of the off-diagonal terms of the density matrix, we write

$$\rho_{12}=\tilde{\rho}_{12}e^{i\omega t},$$

$$\rho_{21}=\tilde{\rho}_{21}e^{-i\omega t}. \tag{4}$$

Putting this into E_{MNP}, we have

$$E_{\mathrm{MNP}}=\left(\frac{E_0}{2}+\frac{1}{4\pi\epsilon_B}\frac{s_\alpha\mu}{\epsilon_{\mathrm{effS}}R^3}\tilde{\rho}_{21}\right)e^{-i\omega t}+\left(\frac{E_0}{2}+\frac{1}{4\pi\epsilon_B}\frac{s_\alpha\mu}{\epsilon_{\mathrm{effS}}R^3}\tilde{\rho}_{12}\right)e^{i\omega t}.$$

Returning to P_{MNP},

$$P_{\mathrm{MNP}}=(4\pi\epsilon_B)a^3\left[\gamma\left(\frac{E_0}{2}+\frac{1}{4\pi\epsilon_B}\frac{s_\alpha\mu}{\epsilon_{\mathrm{effS}}R^3}\tilde{\rho}_{21}\right)e^{-i\omega t}+\gamma^*\left(\frac{E_0}{2}+\frac{1}{4\pi\epsilon_B}\frac{s_\alpha\mu}{\epsilon_{\mathrm{effS}}R^3}\tilde{\rho}_{12}\right)e^{i\omega t}\right].$$

We can now write the field acting on the SQD as,

$$E_{\mathrm{SQD}}=\frac{\hbar}{\mu}\{(\Omega+G\tilde{\rho}_{21})e^{-i\omega t}+(\Omega^*+G^*\tilde{\rho}_{12})e^{i\omega t}\}, \tag{5}$$

where we have defined

$$G=\frac{s_\alpha^2\gamma a^3\mu^2}{4\pi\epsilon_B\hbar\epsilon_{\mathrm{effS}}^2R^6},$$

$$\Omega=\frac{E_0\mu}{2\hbar\epsilon_{\mathrm{effS}}}\left(1+\frac{\gamma a^3 s_\alpha}{R^3}\right).$$

G arises when the applied field polarizes the SQD, which in turn polarizes the MNP and then produces a field to interact with the SQD. Thus, this can be thought of as the self-interaction of the SQD because this coupling to the SQD depends on the polarization of the SQD. The first term in Ω is just the direct coupling to the applied field and the second term is the field from the MNP that is induced by the applied field.

We solve the master equation

$$\dot{\rho}=\frac{i}{\hbar}[\rho,\mathcal{H}_{\mathrm{SQD}}]-\Gamma(\rho), \tag{6}$$

where $\Gamma(\rho)$ is the relaxation matrix with entries $\Gamma_{11}=\frac{\rho_{11}-1}{\tau_0}$, $\Gamma_{12}=\Gamma^*_{21}=\frac{\rho_{12}}{T_{20}}$ and $\Gamma_{22}=\frac{\rho_{22}}{\tau_0}$. The relaxation time τ_0 contains a contribution from nonradiative decay to dark states. We now write the density-matrix elements as

$$\tilde{\rho}_{12}=A+iB,$$

$$\tilde{\rho}_{21}=A-iB,$$

$$\Delta = \rho_{11} - \rho_{22},$$

where Δ is the population difference between the excited and ground states. To solve Eq. (6), we make the rotating wave approximation. When changing the Hamiltonian to the interaction picture we keep terms that oscillate like $e^{i(\omega-\omega_0)t}$ and neglect terms that oscillate like $e^{i(\omega+\omega_0)t}$. Making use of our definitions and the rotating wave approximation, we come to the set of coupled differential equations,

$$\dot{A} = -\frac{A}{T_{20}} + (\omega - \omega_0)B - (\Omega_I + G_I A - G_R B)\Delta,$$

$$\dot{B} = -\frac{B}{T_{20}} - (\omega - \omega_0)A - (\Omega_R + G_R A + G_I B)\Delta,$$

$$\dot{\Delta} = \frac{1-\Delta}{\tau_0} + 4\Omega_I A + 4\Omega_R B + 4G_I(A^2 + B^2), \tag{7}$$

where G_R, G_I, Ω_R and Ω_I are the real and imaginary parts of G and Ω, respectively. These equations differ from those arrived at previously[10,11] in the signs of several terms. Previously, the positive and negative contributions of the electric field were not properly separated. The sign differences have little effect except at strong fields and strong coupling.

In the steady-state limit we set the left hand side of Eq. (7) to zero. Due to the nonlinear nature of these equations, more than one steady state solution can exist for certain values of the parameters. In these regions we must solve the full set of dynamical Eq. (7), allowing them to evolve from the initial conditions for times on the order of 10 ns to reach the steady state. This allows us to identify the dependence of the steady state on the starting conditions. Except where noted, evolution for 10 ns was sufficient to reach steady state in cases we considered.

A. Energy

The rate at which energy is absorbed by our system consists of two parts, Q_{SQD} and Q_{MNP}. The SQD absorbs energy by the creation of an exciton followed by a nonradiative decay. The rate is just $Q_{\mathrm{SQD}} = \hbar\omega_0\rho_{22}/\tau_0$. To calculate the energy absorbed by the MNP, we take the time average of the volume integral, $\int \mathbf{j}\cdot\mathbf{E}dv$, where $\mathbf{j}$ is the current density and $\mathbf{E}$ is the electric field inside the MNP. The electric field incident on the MNP is the applied field plus the field due to the polarization of the SQD,

$$\begin{aligned} E_{\mathrm{MNP}}^{(outside)} &= E + \frac{1}{4\pi\epsilon_B}\frac{s_\alpha \mu}{\epsilon_{\mathrm{effS}} R^3}(\rho_{12} + \rho_{21}) \\ &= \left(E_0 + \frac{s_\alpha \mu A}{2\pi\epsilon_B \epsilon_{\mathrm{effS}} R^3}\right)\cos(\omega t) - \frac{s_\alpha \mu B}{2\pi\epsilon_B \epsilon_{\mathrm{effS}} R^3}\sin(\omega t) \\ &= E_C \cos(\omega t) - E_S \sin(\omega t), \end{aligned} \tag{8}$$

where

$$E_C = E_0 + \frac{s_\alpha \mu}{2\pi\epsilon_B \epsilon_{\mathrm{effS}} R^3} A$$

is the component of the field that is in phase with the applied field and

$$E_S = \frac{s_\alpha \mu}{2\pi\epsilon_B \epsilon_{\mathrm{effS}} R^3} B$$

is 90° out of phase with the applied field. Separating the positive and negative frequency parts of the field, we can write the field inside the MNP as

$$E_{\mathrm{MNP}}^{(\mathrm{inside})} = \frac{E_C - iE_S}{2\epsilon_{\mathrm{effM}}} e^{-i\omega t} + \frac{E_C + iE_S}{2\epsilon_{\mathrm{effM}}^*} e^{i\omega t},$$

where $\epsilon_{\mathrm{effM}} = \frac{2\epsilon_B + \epsilon_M}{3\epsilon_B}$.

We calculate the current density of the MNP from the derivative of its polarization, P_{MNP}. Written in terms of E_C and E_S, P_{MNP} is

$$P_{\mathrm{MNP}} = 2\pi a^3 \epsilon_B [\gamma(E_C - iE_S)e^{-i\omega t} + \gamma^*(E_C + iE_S)e^{i\omega t}].$$

Since we are assuming that we have factored out the fast varying part of the density matrix in Eq. (4), we take the time derivatives of A and B to be zero and we then have for the current density, j,

$$j = \frac{2\pi i\omega\epsilon_B a^3}{\mathcal{V}}(\gamma^*(E_C + iE_S)e^{i\omega t} - \gamma(E_C - iE_S)e^{-i\omega t}),$$

where $\mathcal{V}$ is the volume of the MNP.

We can now calculate $Q_{\mathrm{MNP}}(t)$,

$$\begin{aligned} Q_{\mathrm{MNP}}(t) &= \int \mathbf{j}\cdot\mathbf{E}dv \\ &= i\pi\epsilon_B \omega a^3 \left[\frac{\gamma^*}{\epsilon_{\mathrm{effM}}}(E_C + iE_S)^2 e^{2i\omega t} - \frac{\gamma}{\epsilon_{\mathrm{effM}}^*}\right. \\ &\quad \times (E_C + iE_S)^2 e^{-2i\omega t} - 2i\,\mathrm{Im}\left[\frac{\gamma}{\epsilon_{\mathrm{effM}}^*}\right] \\ &\quad \left. \times (E_C + iE_S)(E_C - iE_S)\right]. \end{aligned}$$

Taking the time average of this result over the period of fast oscillation yields Q_{MNP},

$$Q_{\mathrm{MNP}} = 2\pi\epsilon_B \omega a^3\,\mathrm{Im}\left[\frac{\gamma}{\epsilon_{\mathrm{effM}}^*}\right](E_C^2 + E_S^2). \tag{9}$$

Thus, E_C and E_S are key in determining the shape of the response. Since E_S is out of phase with the applied field, it will typically be substantially smaller than E_C. However, for the strongest coupling that we will look at, E_C and E_S are comparable.

B. Numerical calculations in the large field limit

In this paper we will consider the large field limit as defined in Ref. 10 (intensity of 10^3 W/cm^2) with E parallel to the axis of our SQD-MNP molecule, i.e., $s_\alpha = 2$ and we take

the dielectric constant of the background to be $\epsilon_B = \epsilon_0$. In this limit, most of the energy of the system is concentrated in the MNP so our focus will be on the field felt by the MNP. However, at strong coupling, the self-interaction of the SQD is relatively large and thus becomes important in determining the behavior of the system.

For the MNP, we take $\epsilon_M(\omega)$ as the bulk dielectric constant of gold as found experimentally.[20] For a small, spherical, gold MNP, the response has a broad plasmon peak near 2.4 eV with a width of approximately 0.25 eV. We let the radius of the MNP vary between 3 and 8 nm.

For the SQD, we take the relaxation times to be $\tau_0 = 0.8$ ns and $T_{20} = 0.3$ ns, and we take $\epsilon_S = 6\epsilon_0$. For the exciton resonant frequency we take it to be 2.5 eV which is near the broad plasmon frequency of gold. For the MNP size regime we consider, the plasmon resonance for a sphere varies little with particle size. However, the size, shape, and material of the SQD strongly determine both the exciton energy level and its dipole moment. In this paper, we consider the simplest model and ignore this size dependence. While this is clearly an oversimplification, it allows us to identify the range of optical signatures which are possible in the strong-field limit. Recent measurements of SQD dipole moments have yielded values of ≈ 1 e nm for self-assemble QDs (Ref. 21) and several times that for interface fluctuation QDs.[22] For the dipole moment of the SQD, we let it vary between 0.25 and 6.0 e nm, corresponding to a SQD size of 2–30 nm. For the purposes of this investigation, this range is a reasonable coverage of the observed values that allows us to test the full spectrum of behavior.

By manipulating a and μ, which are effectively the sizes of the MNP and SQD respectively, we can change the relative strengths of the local fields and, in turn, the strengths of the three different couplings (G and the two terms that make up Ω). Looking at the solutions to the differential equations, Eq. (7), both dynamically and in the steady state limit, we find four distinct regimes of behavior in the a vs μ parameter space (see Fig. 2).

Regions I and II are discussed in detail in Ref. 11 but we give a brief overview here for completeness. Included in this overview we provide distinct insight gleamed from viewing the exciton in the system as a damped driven harmonic oscillator. We then focus our attention on the transition regime between regions II and III, in which we find a suppression in the response of the SQD. Finally, we take another look at region III, which we addressed previously in Ref. 11 but we are now able to more fully describe its behavior using this driven harmonic oscillator model.

III. REGIONS I AND II

Region I is the regime of weakest coupling between the SQD and MNP discussed extensively in Ref. 10 and again in Ref. 11. In the strong field limit, the exciton is strongly driven at resonance, overcomes the damping, and the population difference, Δ, is zero. The energy absorption spectrum of the MNP displays an asymmetrical Fano shape (see Fig. 3). It occurs when there is interference between the applied field and the induced field produced by the SQD at the MNP.

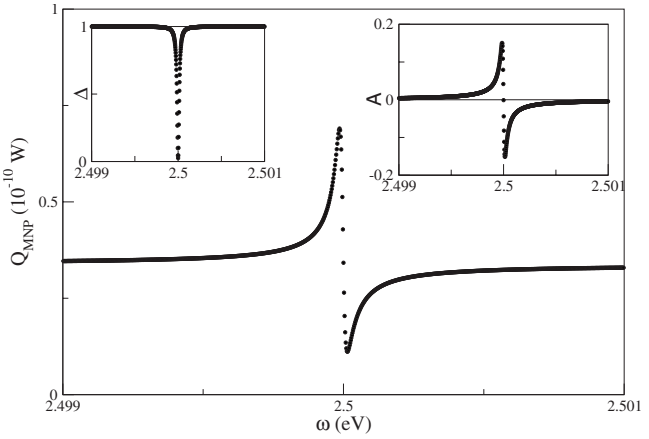

FIG. 3. Region I. $R = 13$ nm, $a = 3$ nm, $\mu = 0.25$ e nm. Absorption rate of the MNP, Q_{MNP}, shows a Fano shape in the response due to the phase change in dipole moment of the SQD. This phase change is shown in the real part of the SQD dipole moment in the right inset. Left inset shows the sharp dip in the population difference at resonance.

In this region, the dominant component of the field acting on the MNP is E_C, with E_S being negligible at weak coupling. It is important to note that in region I, E_C is dominated by the applied field. Although there is interference, E_0 is always greater than $\frac{s_\alpha \mu}{2\pi\epsilon_B \epsilon_{effS} R^3} A$ (in region II, the local field can be larger than the driving field). The interference changes from constructive to destructive at resonance where the sign of A changes (see Fig. 3). Below resonance A is positive and above resonance it is negative. Since A is the real part of the SQD dipole moment it determines the phase of the local field acting on the MNP. Thus, below resonance the local field is in phase with the applied field and above resonance the local field is 180° out of phase with the applied field. This phase change is a common feature of a damped driven oscillator.

When the coupling is increased by increasing μ, the character of the Fano response becomes more complicated. Region II is characterized by the additional peak that appears in the Fano line shape of region I (see Fig. 4). This second peak occurs where the minimum of E_C in Eq. (9) crosses through zero (in this region of parameter space, E_S is still an order of magnitude smaller). For this sign change to occur, the magnitude of the local field, $\frac{s_\alpha \mu}{2\pi\epsilon_B \epsilon_{effS} R^3} A$, must be larger than the applied field, E_0, over a range of frequencies and must be out of phase with E_0 over these frequencies. As a consequence, E_C changes sign just above resonance (the dip in Fig. 4). E_C changes sign again, well above resonance (the barely visible second dip in Fig. 4), when the induced local field again becomes weaker than the applied field. When E_C changes sign at these two locations, the field on the MNP is nearly completely canceled and the metal becomes reflective. The absorption remains finite only because the small out-of-phase component E_S is nonzero. Because this is an interference effect between the driving field and the field produced by the SQD, this is an EXIT in the MNP that is due to the phase change at resonance of the driven SQD oscillator.

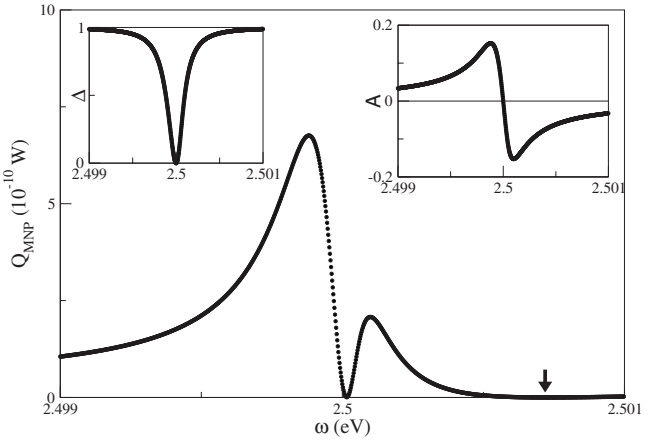

FIG. 4. Region II. $R=13$ nm, $a=3$ nm, $\mu=2$ e nm. Absorption rate of the MNP, Q_{MNP}, shows an exciton-induced transparency due to the phase change in the dipole moment of the SQD when the local field incident on the MNP from the SQD is larger than the applied field. Right inset shows the real part of the SQD dipole moment which undergoes a phase change at resonance. Left inset shows the dip in the population difference at resonance. All three plots show a general broadening relative to region I. The arrow indicates the second dip in Q_{MNP}.

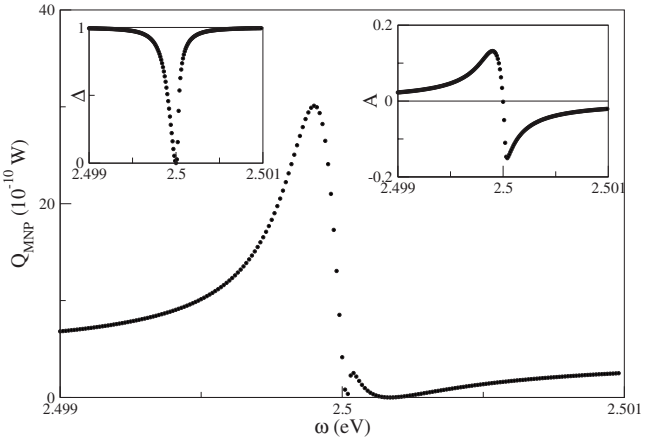

FIG. 5. Weak suppression. $R=13$ nm, $a=7$ nm, $\mu=1$ e nm. Here we see the beginning of the suppression in the response of the SQD, apparent in a slight asymmetry in Δ. $\Gamma_b=98$ μeV, $\Gamma_a=37$ μeV, $S=2.65$.

IV. TRANSITION REGION: SUPPRESSION

In regions I and II, interference between the applied field and the induced field due to the polarization of the SQD caused a phase shift in the net electric field incident on the MNP at resonance and an asymmetry in the response of the MNP. However, this asymmetry is not manifested in the response of the SQD, i.e., Δ, (see Fig. 4, for example) because the SQD does not couple directly to the field produced by the polarization of the SQD. However, this field does couple to the MNP, which in turn polarizes and produces a field that couples to the SQD. This self-interaction of the SQD is G in Eq. (5). If the self-interaction becomes significant, there will also be non-negligible interference of the electric fields at the SQD. The interference then can suppress or enhance the response of the SQD.

The transition region is characterized by this suppression of the response of the SQD above resonance. To measure the extent of the suppression, we measure the width of Δ, both above and below resonance at half maximum (half width, half max). We label these two half widths, Γ_a and Γ_b, for above and below resonance respectively. We then define the suppression factor, S, to be ratio of these two widths, $S=\Gamma_b/\Gamma_a$. We choose $S=2$ to define the boundary of the suppression region. However, note that the characteristic double peaked EXIT structure still exists for S values greater than 2. The double peak structure of region II disappears only once the suppression becomes so strong that the response function becomes discontinuous.

For a fixed value of the MNP radius ($a=7$ nm) and with a small value of the SQD dipole moment scalar ($\mu=1$ e nm), we see the beginning of the suppression above resonance ($S=2.65$). The population difference, Δ, is continuous as is the SQD dipole moment (see Fig. 5).

To see how the suppression develops, we need to look at the composition of the electric field that is incident on the SQD. The field felt by the SQD, [Eq. (5)], is composed of two parts, $\rho_{12}G$ and Ω. Ω consists of the direct coupling to the applied field, E, as well as the response of the MNP to the applied field. The self-interaction term scales as $\sim\mu^2a^3$ and the response of the MNP to the applied field scales as $\sim\mu a^3$. As μ is increased, the self-interaction becomes a significant contribution to the total field (see Fig. 6). For weak suppression, $a=7$ nm, $\mu=1$ e nm (as in Fig. 5) we see that the self-interaction is an order of magnitude smaller than Ω. Because the phase of the self-interaction depends on the phase of ρ_{12}, we again have interference, this time at the SQD between the self-interaction and the driving field (including the indirect contribution through the MNP).

As μ is increased to 2 e nm we see the above resonance suppression grows so strong ($S=72.3$) that it forces a discontinuity in response of the MNP and the diagonal density-matrix elements, as well as in the off-diagonal elements (the

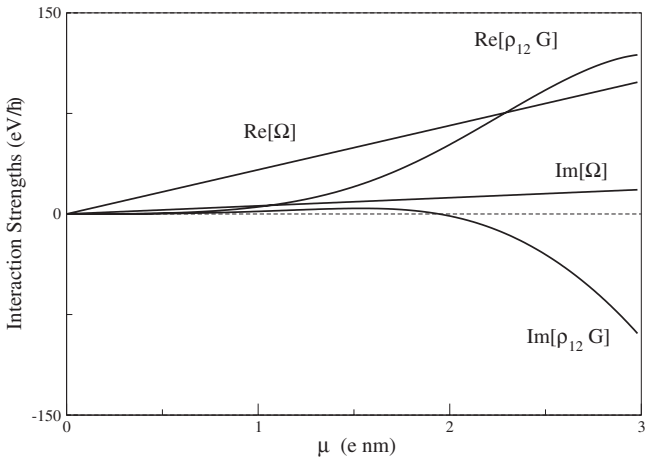

FIG. 6. The relative strengths of the two main interactions that drive the SQD. $\rho_{12}G$, the self-interaction, and Ω, the applied field and the MNP response to the applied field, vs μ for fixed MNP radius ($a=7$ nm) and frequency ($\omega=2.5$ eV). Note: G and Ω are nearly constant over the range of frequencies that we are interested in due to the broad plasmon peak.

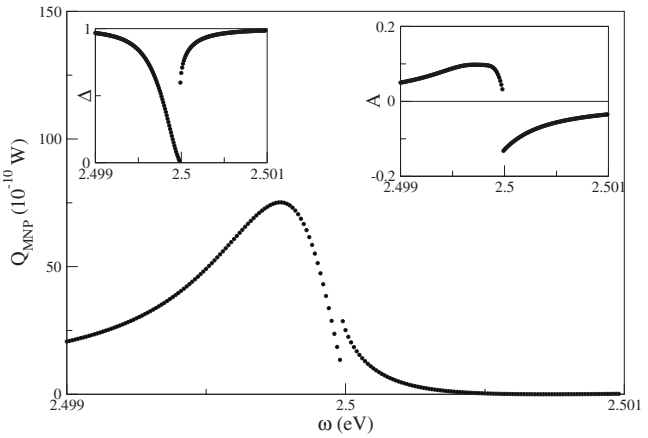

FIG. 7. Strong suppression. $R=13$ nm, $a=7$ nm, $\mu=2$ e nm. Here the suppression has grown large enough that a discontinuity has developed in the diagonal and off-diagonal density-matrix elements as well as the energy absorption of the MNP. $\Gamma_b=217$ μeV, $\Gamma_a=3$ μeV, $S=72.3$.

dipole moment of the SQD) (see Fig. 7). In this regime of strong suppression, we see that the self-interaction is of the same order of magnitude as Ω (see Fig. 6).

As μ is further increased, the suppression increases along with the discontinuity, and the resonance of the SQD begins to shift to lower energies. The location of phase change in ρ_{12} also splits based on the initial conditions of the system (see Fig. 9 and Sec. IV B), much like we see in region III (which will be discussed in Sec. V). Further increase in μ results in further shifts to the resonance of the SQD. This causes the suppression to eventually disappear. The discontinuity however, remains locked in for certain initial conditions, forming what we have previously called region III. As we will see in Sec. V, at $\mu=3.5$ e nm, which is just inside region III, S is reduced to 1.69.

A. Understanding the interference: Phasors and interaction strengths

To understand these interference effects, we first consider a case of weak coupling (small μ). For weak coupling, Ω is much larger than G and we can ignore the effect of G (see Fig. 6). Thus our resultant field on the SQD is mostly in the direction of Ω which is along the real axis both above and below resonance (see Fig. 8). This has the effect of driving the SQD mostly by the real field, i.e., the SQD couples more strongly to A than to B.

However, when the coupling is increased so that G is no longer negligible, the field the SQD sees from the self-coupling is $\rho_{12}G$. Below resonance, $\rho_{12}G$ is in phase with the applied field, but above resonance, it is out of phase with the applied field. The SQD sees a weaker overall field above resonance than below resonance (where $\rho_{12}G$ and Ω remain relatively in phase) and the SQD response is suppressed above resonance.

Because G is more rotated in the complex plane than Ω, the introduction of G also has the effect of rotating the net electric field on the SQD toward the imaginary axis, 90° out

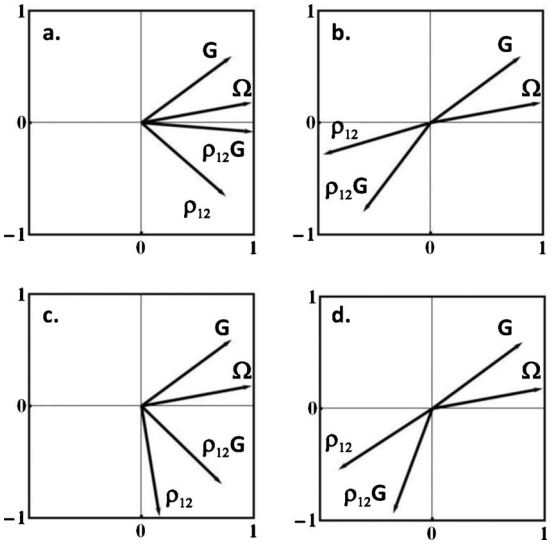

FIG. 8. Depiction of phasors in the complex plane for $a=7$ nm. [(a) and (b)] $\mu=2$ e nm. Suppression region. (a) below resonance ($\omega=2.4999$ eV) and (b) above resonance ($\omega=2.5001$ eV). [(c) and (d)] $\mu=3$ e nm. Region III. (c) below resonance ($\omega=2.4996$ eV) and (d) above resonance ($\omega=2.4999$ eV) (note: resonance has shifted to 2.49915 eV at this point). The phase of G and Ω are nearly constant. Moving left to right (i.e., below to above resonance), we see the real part of ρ_{12} changes sign. This is the phase shift associated with a damped, driven harmonic oscillator.

of phase with the applied field. This allows a stronger coupling to B, the imaginary component of the SQD dipole. The increase in B, causes a further shift in $\rho_{12}G$ toward the negative imaginary axis. This, in effect, decreases the phase difference in the effective field above and below resonance, shutting off the suppression. Looking at Fig. 8 and comparing the two diagrams on top, we see that the phase difference between $\rho_{12}G$ above and below resonance is $\approx 120°$. When the self-coupling becomes stronger (bottom two diagrams), we see the phase angle between $\rho_{12}G$ above and below resonance is smaller ($\approx 60°$).

B. Phase change in ρ_{12}

When the coupling is strong enough to form a discontinuity in the response, the location of the phase change in ρ_{12} becomes dependent on the initial conditions of the system. For $a=5.8$ nm, $\mu=4$ e nm this shift in the crossing at $t=10$ ns is approximately 0.2 meV (see Fig. 9).

To find the location of this phase shift, we begin with our steady-state equations [Eq. (12)]. At the phase change, $A=0$, and we have the system of equations

$$0 = B\Delta G_R + B(\omega - \omega_0) - \Delta\Omega_I,$$

$$0 = -\Delta G_I B - \frac{B}{T_{20}} - \Delta\Omega_R,$$

$$0 = 4G_I B^2 + 4\Omega_R B + \frac{1-\Delta}{\tau_0}. \tag{10}$$

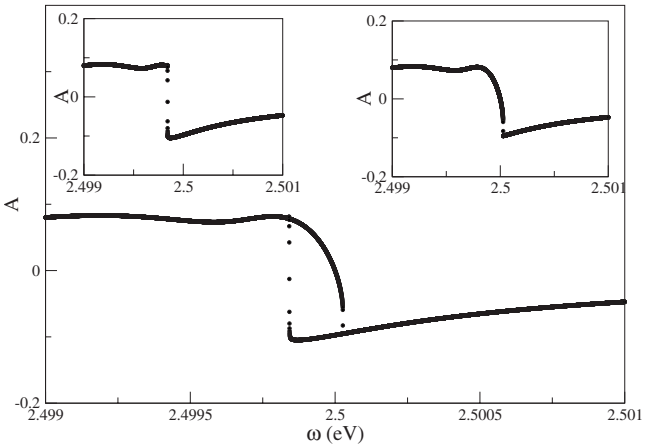

FIG. 9. A, the real part of the SQD dipole moment for $\mu=4$ e nm, $a=5.8$ nm at $t=10$ ns. Left inset: the system starts in the ground state. Right inset: the system starts in a mixed state, $\Delta=0$. Center: an overlay of the two. The location of the phase crossing for the SQD dipole moment is dependent on the initial conditions.

Solving the first for B, we have

$$B = \frac{\Delta\Omega_I}{\omega - \omega_0 + \Delta G_R}.$$

Solving the second for Δ

$$\Delta = -\frac{\Omega_I + \Omega_R T_{20}(\omega - \omega_0)}{T_{20}(G_I\Omega_I + G_R\Omega_R)}.$$

Inserting these results in the third equation yields,

$$0 = \frac{4(G_I\Omega_I + G_R\Omega_R)[\Omega_I + \Omega_R T_{20}(\omega - \omega_0)]}{[G_R + G_I T_{20}(\omega_0 - \omega)]^2} + \frac{(G_I T_{20} + 1)\Omega_I + T_{20}(G_R + \omega - \omega_0)\Omega_R}{T_{20}\tau_0(G_I\Omega_I + G_R\Omega_R)}. \quad (11)$$

This is a cubic equation in $\omega-\omega_0$. In general, for the steady state, we will have either three real solutions, or one real and two complex solutions. For example, we plot the roots of this equation for a fixed value of $\mu=4$ e nm, letting a vary, in Fig. 10. When $a>6.3$ nm, we do in fact have three real solutions (see top of Fig. 10). For $a<6.3$ nm, the only real solution is $\omega-\omega_0=0$.

Looking again at Fig. 9, it appears that for $\mu=4$ e nm, $a=5.8$ nm, there are in fact at least two distinct locations where A can change sign at $t=10$ ns, even though only one crossing is predicted for steady state. When we take the calculation to larger times, we see that not only is there a slight shift in the location of the crossing for the mixed state initial condition but that the crossing becomes increasing sharp and in the steady-state limit ($t\to\infty$) this crossing becomes a discontinuous jump (see bottom of Fig. 10). There is a second location where A can undergo a sign change. However, at this second location, in the steady state, A is not equal to zero.

When all three solutions to Eq. (11) are real, working backward, we see that we have then three real solutions of A, B, and Δ. This is exactly how we have defined region III

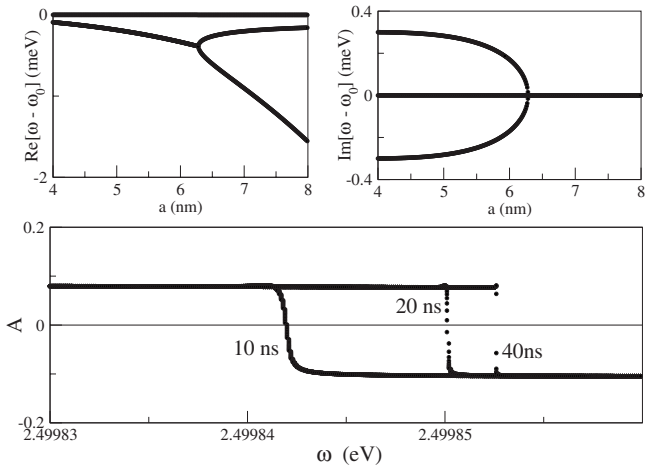

FIG. 10. (Top) The real and imaginary parts, respectively, of solution to the cubic equation that determines the frequency at which A changes sign (plotted for $\mu=4$ e nm). Up to $a=6.3$ nm, there is one real solution and two complex solutions (which are conjugates of each other). In this region, the only real solution is $\omega-\omega_0=0$. For $a>6.3$ nm, three real solutions exist. (Bottom) The real part of SQD dipole moment for $\mu=4$ e nm, $a=5.8$ nm, plotted for 10 ns, 20 ns and 40 ns evolutions, respectively. We see that although for finite time, A has a continuous crossing through zero, as the system evolves to the steady state, the crossing becomes discontinuous.

previously, and we let this condition on the solutions to Eq. (11) determine the boundary between the transition region and region III.

V. REGION III

When the coupling is increased further by increasing both μ and a, a region of bistable response emerges (region III). In this limit, the field that is produced by the SQD and then reflected off the MNP and back onto the SQD (the self-interaction of the SQD) is sufficiently strong to induce a significant contribution to the out of phase component of the density matrix, B, and thus E_S. This stronger coupling to the imaginary part of ρ_{12} is due to the phasor of G being more rotated in the complex plane than that of Ω (as previously discussed). Thus there is a non-negligible value of Q_{MNP} even when $E_C=0$. This, combined with a general broadening due to the increased field strength, can cause the double peaked EXIT structure to disappear.

Most importantly, region III is characterized by bistability in the steady-state solutions. For the same values μ and a, different initial conditions of ρ lead to different steady states (see Fig. 11). This bistability only exists near the resonance frequency of the SQD, away from resonance all initial conditions lead to identical steady states. For $R=13$ nm, $a=7$ nm, and $\mu=3.5$ e nm the width of bistability is 0.25 meV for the mixed state initial conditions $[A(0)=0, B(0)=0, \Delta(0)=0]$ (see Fig. 11). As the values of a and μ get closer to the transition region, this window in ω space shrinks.

Calculation of the resonance shift

As the coupling between the SQD and the MNP is increased and the transition is made into region III, there is a

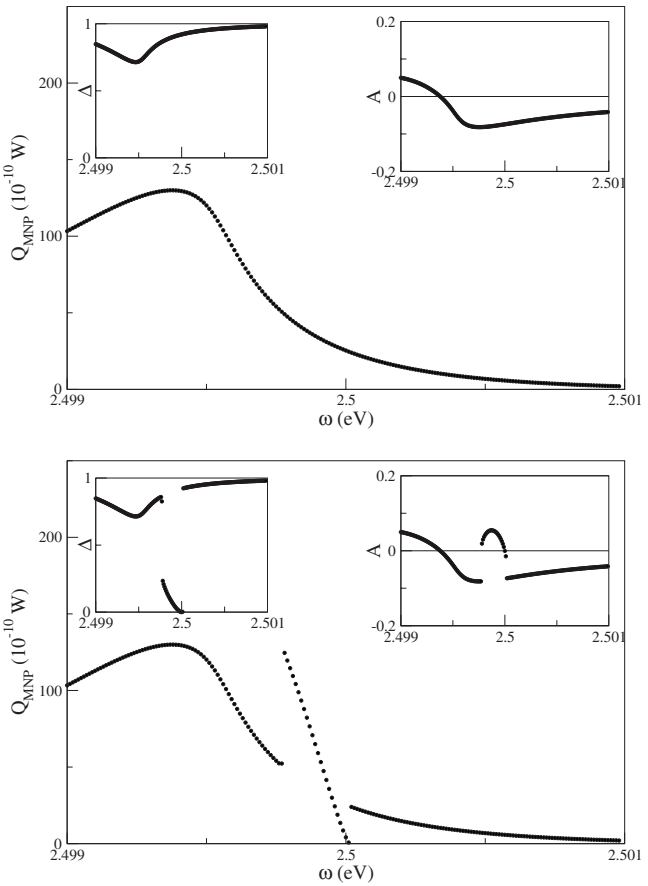

FIG. 11. Region III. $a=7$ nm, $\mu=3.5$ e nm. Coupling to the imaginary part of $\rho_{12}G$ destroys most of the suppression. $\Gamma_b=0.49$ meV, $\Gamma_a=0.29$ meV, $S=1.69$. (top) System is initially in the ground state. (Bottom) System starts in a mixed state. Here we see the bistability of the system, where different initial conditions lead to distinct steady state solutions. We also note the three location where A changes sign, as predicted in the previous section.

redshift in the resonance of the SQD. Accompanied with this redshift, there is a broadening and a decrease in the response of the SQD, i.e., Δ at resonance is no longer nearly 0 (see Fig. 11 for an example of both of these effects).

We can model both the redshift and the new minimum of Δ. Starting with Eq. (7), we set the left-hand side to zero to arrive at the steady state equations. Taking the first two equations and solving for A and B in terms of Δ we have

$$A = -\Delta\left(\frac{k\Omega_I + \delta\omega\Omega_R}{k^2 + \delta\omega^2}\right),$$

$$B = -\Delta\left(\frac{k\Omega_R - \delta\omega\Omega_I}{k^2 + \delta\omega^2}\right),$$

$$\Delta = 1 + \tau_0[4\Omega_I A + 4\Omega_R B + 4G_I(A^2 + B^2)], \tag{12}$$

where we have defined

$$k = \Delta G_I + \frac{1}{T_{20}},$$

$$\delta\omega = \omega - \omega_0 + \Delta G_R.$$

We now take the derivative with respect to ω for each of the equations in Eq. (12). To find the minimum of Δ, we evaluate them at the critical point $\omega=\omega_c$ and set $\Delta'(\omega_c)=0$,

$$A' = \Delta\left[\frac{2\delta\omega k\Omega_I - (k^2 - \delta\omega^2)\Omega_R}{(k^2 + \delta\omega^2)^2}\right], \tag{13}$$

$$B' = \Delta\left[\frac{2\delta\omega k\Omega_R + (k^2 - \delta\omega^2)\Omega_I}{(k^2 + \delta\omega^2)^2}\right], \tag{14}$$

$$\Delta' = \tau_0[4\Omega_I A' + 4\Omega_R B' + 8G_I(AA' + BB')] = 0. \tag{15}$$

Note that G and Ω are nearly constant over the range of frequencies that we consider because the plasmon peak is broad in comparison, thus we take their derivatives with respect to ω to be zero. Putting Eqs. (13) and (14) into Eq. (15), and after a bit of algebra, we arrive at the result

$$0 = \Delta_c\delta\omega,$$

where $\Delta_c \equiv \Delta(\omega_c)$. Δ_c cannot take a value of zero in the steady state, except in the limit that $\tau_0 \to \infty$ (this is easy to check), so we must have $\delta\omega=0$. Using this result, we find that at $\omega=\omega_c$ we have $A=-\Delta_c\frac{\Omega_I}{k}$ and $B=-\Delta_c\frac{\Omega_R}{k}$. Then,

$$\Delta_c = 1 - 4\frac{\tau_0(\Omega_R^2 + \Omega_I^2)}{G_I}\left(\frac{\Delta_c G_I}{k} - \frac{\Delta_c^2 G_I^2}{k^2}\right).$$

Note, that the only assumption we have made thus far is that the steady state exists. To proceed further, we now look at the region of parameter space where the resonance frequency shifts relative to the natural frequency ω_0. Since we are interested in the case in which a shift is seen in the resonance frequency (recalling that this coincides with Δ no longer being nearly zero), we take Δ_c to have a value greater than 0.01 and we have that $1/T_{20}\Delta_c G_I < 1$. Thus, we can expand k^{-1} and k^{-2}. In this case, we have

$$\Delta_c \approx 1 - 4\frac{\tau_0(\Omega_R^2 + \Omega_I^2)}{T_{20}G_I^2\Delta_c}.$$

Solving this quadratic equation for Δ_c and expanding the square root of the discriminant we have

$$\Delta_c \approx 1 - 4\frac{\tau_0(\Omega_R^2 + \Omega_I^2)}{T_{20}G_I^2} + \cdots. \tag{16}$$

So, our resonance occurs at

$$\omega_c = \omega_0 - G_R\left[1 - 4\frac{\tau_0(\Omega_R^2 + \Omega_I^2)}{T_{20}G_I^2}\right]. \tag{17}$$

Using these approximations for Δ_c and ω_c, for typical parameters $\mu=4$ e nm and $a=7$ nm, our approximations give $\Delta_c=0.84$ and $\omega_c-\omega_0=-0.82$ meV. Solving the differential equations numerically we find these two quantities to be $\Delta_c=0.81$ and $\omega_c-\omega_0=-0.79$ meV, respectively, in good agreement with our approximations.

Looking at our expressions that describe the redshift and the minimum of Δ, we see that the turning on of these effects

is controlled by the ratio $(\Omega_R^2+\Omega_I^2)/G_I^2$. Recalling the previous section, we note that this ratio will largely determine the strength of the coupling to the imaginary component of the SQD dipole moment, B, with respect to the coupling to A. An increase in the coupling to the imaginary part of the SQD dipole moment (which has a damping effect on the system) causes not only the suppression to turn off (as we saw previously) but also the redshift and broadening in the SQD resonance and a weakening in response of the SQD.

VI. CONCLUDING REMARKS

To summarize, we have found a transition between the EXIT and the regime of bistability that exists in hybrid MNP SQD systems when they are strongly coupled. In particular, we see a discontinuous jump in response of the system (in both the diagonal and off-diagonal density-matrix elements) and the response of the SQD is highly suppressed above resonance in this transition region. This suppression comes about because the response of the SQD is that of a driven, damped harmonic oscillator. Specifically, this behavior is seen in the response of SQD dipole moment. As in the case of the classical damped driven oscillator, the behavior of the system is determined by the whether the driving frequency is above or below the resonance frequency of the system. Below resonance the dipole moment of the SQD is in phase with the driving field, and above resonance it is 180° out of phase. Since the phase of the self interaction of the SQD is determined by the phase of its own dipole moment, there is destructive interference above resonance and constructive interference below resonance, between the applied field and the self-interaction field. Furthermore, coupling to the imaginary part of the SQD dipole moment largely determines whether EXIT, suppression or bistability in the system is visible. This in itself provides an avenue that could be exploited to engineer systems (both coupling strength and geometry) to bias toward a particular regime of behavior (which we will discuss in a follow-up paper).

*Corresponding author; artuso@umd.edu

[1] D. E. Chang, A. S. Sørensen, P. R. Hemmer, and M. D. Lukin, Phys. Rev. Lett. **97**, 053002 (2006).
[2] M. L. Brongersma, J. W. Hartman, and H. A. Atwater, Phys. Rev. B **62**, R16356 (2000).
[3] T. Pons, I. Medintz, K. Sapsford, S. Higashiya, A. Grimes, D. English, and H. Mattoussi, Nano Lett. **7**, 3157 (2007).
[4] A. Akimov, A. Mukherjee, C. Yu, D. Chang, A. Zibrov, P. Hemmer, H. Park, and M. Lukin, Nature (London) **450**, 402 (2007).
[5] Y. Fedutik, V. V. Temnov, O. Schops, U. Woggon, and M. V. Artemyev, Phys. Rev. Lett. **99**, 136802 (2007).
[6] H. Mertens, J. Biteen, H. Atwater, and A. Polman, Nano Lett. **6**, 2622 (2006).
[7] E. Altewischer, M. P. van Exter, and J. P. Woerdman, Nature (London) **418**, 304 (2002).
[8] P. F. Griffin, K. J. Weatherill, S. G. MacLeod, R. M. Potvliege, and C. S. Adams, New J. Phys. **8**, 11 (2006).
[9] S. Fasel, F. Robin, E. Moreno, D. Erni, N. Gisin, and H. Zbinden, Phys. Rev. Lett. **94**, 110501 (2005).
[10] W. Zhang, A. O. Govorov, and G. W. Bryant, Phys. Rev. Lett. **97**, 146804 (2006).
[11] R. D. Artuso and G. W. Bryant, Nano Lett. **8**, 2106 (2008).
[12] A. Govorov, G. Bryant, W. Zhang, T. Skeini, J. Lee, N. Kotov, J. Slocik, and R. Naik, Nano Lett. **6**, 984 (2006).
[13] H. Xu, X.-H. Wang, M. P. Persson, H. Q. Xu, M. Käll, and P. Johansson, Phys. Rev. Lett. **93**, 243002 (2004).
[14] M.-T. Cheng, S.-D. Liu, H.-J. Zhou, Z.-H. Hao, and Q.-Q. Wang, Opt. Lett. **32**, 2125 (2007).
[15] M. Durach, A. Rusina, V. I. Klimov, and M. I. Stockman, New J. Phys. **10**, 105011 (2008).
[16] J. Lindberg, K. Lindfors, T. Setälä, and M. Kaivola, J. Opt. Soc. Am. A **24**, 3427 (2007).
[17] S. M. Sadeghi, L. Deng, X. Li, and W.-P. Huang, Nanotechnology **20**, 365401 (2009).
[18] L. Landau, E. Lifshitz, and L. Pitaevskii, *Electrodynamics of Continuous Media* (Butterworth-Heinemann, Oxford, 1984).
[19] A. Yariv, *Quantum Electronics* (Wiley, New York, 1975).
[20] P. B. Johnson and R. W. Christy, Phys. Rev. B **6**, 4370 (1972).
[21] K. L. Silverman, R. P. Mirin, S. T. Cundiff, and A. G. Norman, Appl. Phys. Lett. **82**, 4552 (2003).
[22] T. H. Stievater, X. Li, D. G. Steel, D. Gammon, D. S. Katzer, D. Park, C. Piermarocchi, and L. J. Sham, Phys. Rev. Lett. **87**, 133603 (2001).